Ultrafast gain recovery and large nonlinear optical response in submonolayer quantum dots

Benjamin Lingnau* and Kathy Lüdge
Institut für Theoretische Physik, Technische Universität Berlin, Berlin, Germany

Bastian Herzog,† Mirco Kolarczik, Yücel Kaptan, Ulrike Woggon, and Nina Owschimikow
Institut für Optik und Atomare Physik, Technische Universität Berlin, Berlin, Germany
(Received 6 May 2016; revised manuscript received 24 June 2016; published 11 July 2016)

Submonolayer quantum dots combine the zero-dimensional charge-carrier confinement of self-assembled quantum dots with the large density of states of a quantum well. Electroluminescence and pump-probe experiments on a submonolayer-based optical amplifier show that the system exhibits a high gain of 90 cm^{-1} and an ultrafast gain recovery. We propose a rate equation system describing the microscopic carrier dynamics which quantitatively reproduces the observed behavior and provides deeper theoretical understanding of the material system. In contrast to Stranski-Krastanov quantum dots, the fast gain recovery is enhanced by a strong interdot coupling. Optically inactive submonolayer states form an efficient carrier reservoir and give rise to a large nonlinear optical response.

DOI: 10.1103/PhysRevB.94.014305

I. INTRODUCTION

Zero-dimensional (0D) localization centers for carriers assist the radiative recombination of electrons and holes in semiconductors [1]. The concept is well established in a wide range of applications, ranging from the exploration of fundamental issues of light-matter interaction to the use in optoelectronic devices [2–4]. Frequently, the 0D centers are embedded in a solid state matrix, which supplies excitation and scattering channels via its characteristic energy structure. A classical example for 0D confinement are quantum dots (QDs) grown by the Stranski-Krastanov (SK) method, where narrow-band-gap material is deposited on a large-band-gap matrix until it self assembles into lens-shaped agglomerations upon reaching a critical thickness [5]. SK-QDs are the workhorse of QD-based optoelectronics, as they provide a clean, spectrally well-separated ground state (GS) transition and a fast charge-carrier recovery after depletion [6–8]. A drawback of this system, however, is that due to the growth method the areal density that can be achieved is limited. For the In(Ga)As material system it is about 10^{11} cm^{-2}, which implies a massively reduced density of states (DOS) and achievable optical gain per unit length in comparison, e.g., to the two-dimensional (2D) quantum wells (QWs) [9].

For the InAs/GaAs material system, the growth of submonolayer (SML)-based localization centers as In-rich agglomerations in a GaAs matrix promises to combine a large DOS with the favorable properties of QDs [10–13]. Consequently, these devices are expected to provide high optical gain and ultrafast gain recovery. Recently, we have shown that gain and phase recovery in an SML-based optoelectronic device are indeed as fast as observed in SK-QDs, making the system an attractive choice as active medium in optoelectronics [14]. Due to the fast exciton dissociation within the SMLs, they are strong candidates for the application in photodetector and solar cell devices, where the SML medium can lead to a fast and efficient device operation [15,16]. The rather strong phase response of SML devices makes them favorable candidates for nonlinear optical applications employing self or cross-phase modulation.

The theoretical description of SML devices has been the topic of many recent publications. Investigations directed at the dimensionality of carrier confinement in SML structures have revealed the presence of 0D as well as 2D signatures [17–21], in contrast to the strong 0D confinement in SK-QDs. In addition, a lateral coupling between the agglomeration centers has been proposed and is substantiated by eight-band $k * p$ calculations showing a large delocalization in particular of the electron wave function [22].

In this paper, we aim to assemble this information into a consistent picture of the carrier dynamics in and between SML-QDs. To this end, we develop a numerical model allowing predictions of the dynamics and behavior of such structures. We investigate the dynamical properties of InAs-based SML-QDs as active medium in an optoelectronic device in ultrafast pump-probe experiments and quantitatively compare the experimental results with our theoretical model. Our investigations help us to determine the complex density of states of the SML-QDs as well as the carrier dynamics and scattering in such structures. We will highlight the unique properties of the SML-QDs and compare them with conventional SK-QD based devices.

II. SAMPLES AND EXPERIMENT

The investigated device is a semiconductor optical amplifier (SOA) structure containing InAs/GaAs SML-QDs grown by metal organic chemical vapor phase epitaxy. Details of the structure can be found in Appendix A. A schematic of the active region containing the SMLs is shown in Fig. 1(a), right column. The resulting localization centers provide a relatively shallow confinement, as illustrated in the band structure in Fig. 1(b), with in particular the electron wave function being delocalized over many InAs agglomerations, while the hole wave function remains more localized [21]. The electroluminescence (EL) obtained from the device is

*lingnau@itp.tu-berlin.de
†BHerzog@physik.tu-berlin.de

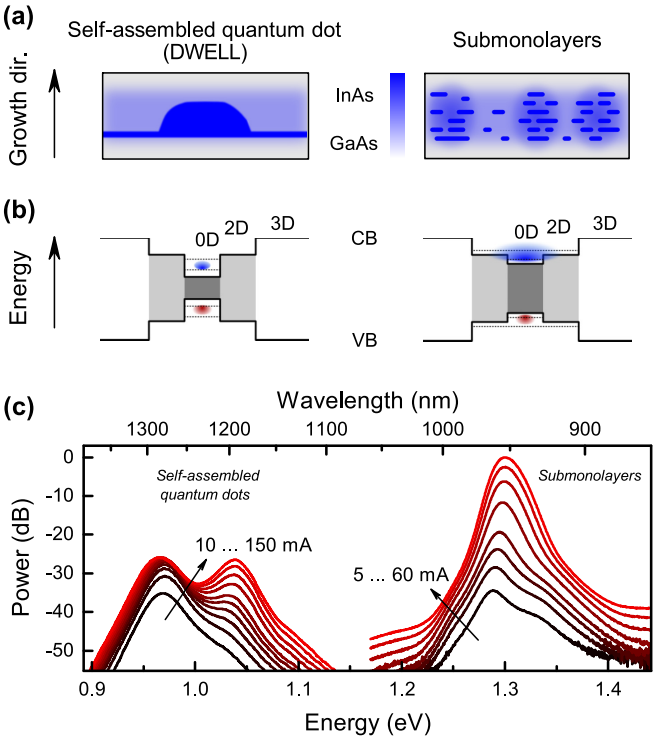

FIG. 1. (a) Illustration of the epitaxial structure of the self-assembled Stranski-Krastanov quantum dots (left) and the submonolayer islands (right). (b) Energy level scheme for the particular active regions, illustrating the confinement for the electron (blue) and hole (red) wave function. CB: conduction band, VB: valence band. (c) Electroluminescence spectra of the particular devices at various injection currents.

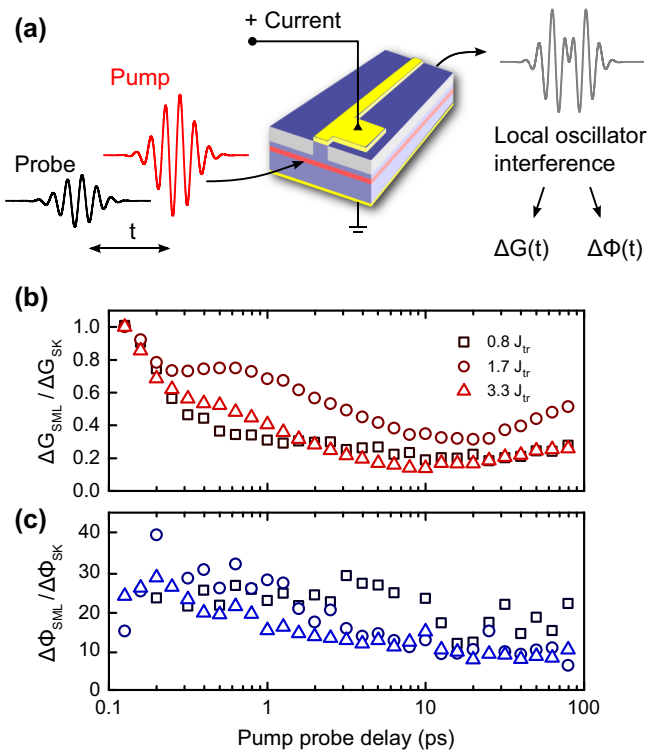

FIG. 2. (a) Illustration of the heterodyne pump-probe experiment. By interference of the probe pulse with a local oscillator pulse the pump-induced changes of gain ΔG (population) and phase $\Delta\varphi$ (refractive index) can be resolved. Ratios of experimental gain (b) and phase (c) recovery dynamics of the SML SOA and the SK-QD SOA at injection currents of $0.8J_{tr}$, $1.7J_{tr}$, and $3.3J_{tr}$ with the transparency current J_{tr}.

centered at 960 nm at low injection current and shows a slight blueshift for higher currents [Fig. 1(c), right panel]. The strong growth of the luminescence (note the logarithmic power axis) promises a high optical gain.

As a reference structure, we use an SOA based on InAs SK-QDs in a dot-in-a-well (DWELL) structure. Details of the device are shown in Appendix A. The DWELL structure is displayed schematically in Figs. 1(a) and 1(b) (left panels). The QD GS is emitting at 1280 nm [Fig. 1(c) left spectra], and the QW is located at 1160 nm [23]. This corresponds to a separation in energy of about 100 meV between the QW reservoir and dot states, ensuring good 0D confinement in the QD GS. Note that for a comparison of carrier dynamics, this relative separation of localization center and continuum is important and not the absolute emission energy.

A schematic of the device and an illustration of the principle of the ultrafast heterodyne-detected pump-probe experiment [24] is shown in Fig. 2(a). The experiment utilizes an interferometric approach to access carrier and phase dynamics in the active region of a waveguide, where pump and probe pulses are transmitted collinear and co-polarized. By interference with a local oscillator pulse on a photodetector, a complex signal $S(t)$ is recorded, from which the differential changes of amplitude and phase of the probe pulse are retrieved. The differential intensity gain is defined as $\Delta G = 20 \times \log(\mathrm{Re}(S)/\mathrm{Re}(S_0))$, and the differential phase as $\Delta\Phi = \mathrm{Im}(S) - \mathrm{Im}(S_0)$, where S_0 corresponds to the signal of the undisturbed system (probe pulse only) and S to the signal after a pump pulse has been applied. The experiment is described in greater detail in Appendix B and in Ref. [25]. Differential gain and phase recovery for the SML-QDs have been published in Ref. [14]. The gain recovery dynamics of the SML-QDs is excellently described by a biexponential function with two time constants differing by two orders of magnitude, with the fast time constant from 2 to 6 ps, and the slow time constant of 600 to 800 ps, respectively. The timescale of the recovery compares favorably with the typical gain recovery rates measured in SK-QDs [26,27], where the crossover from intradot processes to re-equilibration leads to a more complex shape of the gain recovery curve.

To emphasize similarities and differences of differential gain and phase measured in single-color pump-probe experiments in both devices discussed here, we show in Figs. 2(b) and 2(c) the relative gain and phase recovery of the SML device normalized to the SK-QD values. The individual pump-probe traces of both devices are displayed in the numerical analysis part in Sec. III. The experiments were performed at the maximum of the luminescence of the SML-QD SOA at 960 nm and of the SK-QD SOA at 1280 nm for three different multiples of the respective transparency current J_{tr}. The transparency current is determined as the current at which the differential gain trace switches its sign from positive at low

injection currents to negative at high currents. The respective transparency currents were determined to be 13 mA for the SML SOA and 6 mA for the SK-QD SOA.

The direct comparison of the SML gain recovery with our SK-QDs in Fig. 2(b) shows that the fast gain recovery component is more dominant in the SML SOA. The SK-QD SOA generally shows a more complex recovery behavior, reflected in dynamics at an intermediate timescale of 1–10 ps.

The ratios of the differential phase changes accompanying the gain recovery are plotted in Fig. 2(c). For the chosen relatively moderate injection currents the phase response of the SK-QDs is small. The SML-QDs, on the other hand, display a significant phase change upon optical pumping, reflected in consistently large values for $\Delta\Phi_{\mathrm{SML}}/\Delta\Phi_{\mathrm{SK}}$. This strong index change entails a significant nonlinear index response of the SML structure. SK-QDs are known to display a nonlinear refractive index n_2 of up to 10^{-5} cm^2/W, which is comparable to the extreme nonlinear response observed, e.g., in graphene [28,29]. The total n_2 is composed of an intrinsic and a dynamical part, the latter of which is what our experiments detect. The dynamical nonlinear response of the SML-QDs is thus very promising for nonlinear photonics applications.

III. NUMERICAL MODELING AND RESULTS

In this section we will develop a suitable model for the carrier dynamics of both devices starting from the microscopically motivated multilevel rate-equation model used in previous publications to describe SK-QD based SOAs and lasers [30–32]. In order to reduce the degrees of freedom for the model parameters and thus give reliable evidence about the electronic structure of the investigated systems, we generalize the rate equation system as much as possible. At first we develop a suitable model for the EL spectra and the gain- and phase dynamics of the SK-QD SOA, assuming a density of energy states (DOS) in agreement with established literature. Secondly we modify the DOS and scattering processes to fit the numerical results to the measured EL and dynamics of the SML SOA.

A. Self-assembled quantum dots (SK-QDs)

The charge-carrier dynamics of SK-QD amplifier structures is strongly determined by the filling of the active QD states by a common 2D charge-carrier reservoir. In the given DWELL structure, described in Fig. 1(d), the reservoir is formed by the two-dimensional InGaAs QW which supplies charge carriers to the QDs by means of Coulomb Auger scattering [33,34]. Together with the intradot relaxation of carriers from higher excited states to the QD ground state, this efficient capture from the reservoir is responsible for the ultrafast gain recovery of SK-QD SOAs [8,35–37].

In order to accurately model the charge-carrier dynamics, we take into account an energy structure as sketched in Fig. 3. The carrier density in the reservoir N^{res} as well as the occupation probability ρ_m^j in the QD ground and the twofold-degenerate first excited state is described by a set of coupled rate equations. Here, the index $m \in \{\mathrm{GS},\mathrm{ES}\}$ denotes the corresponding quantities for the ground and first excited state, respectively. We separate the QD distribution

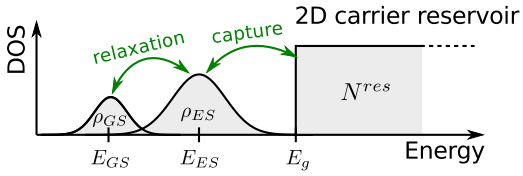

FIG. 3. Sketch of the density of states (DOS) assumed in the SK-QD rate equation model, along with the included scattering channels (arrows).

into different subgroups denoted by an index j, characterized by their respective transition frequencies ω_m^j, to account for inhomogeneous broadening.

$$\frac{\partial}{\partial t}N^{\mathrm{res}} = J - \frac{N^{\mathrm{res}}}{\tau_{\mathrm{res}}} - 4N^{\mathrm{QD}}\sum_j f^j \widetilde{R}_{\mathrm{ES}}^{\mathrm{cap}}(j) \tag{1}$$

$$\frac{\partial}{\partial t}\rho_{\mathrm{ES}}^j = -\frac{\left(\rho_{\mathrm{ES}}^j\right)^2}{\tau_{\mathrm{ES}}} + \widetilde{R}_{\mathrm{ES}}^{\mathrm{cap}}(j) - \frac{1}{2}\widetilde{R}^{\mathrm{rel}}(j) - R_{\mathrm{ES}}^{j,\mathrm{stim}} \tag{2}$$

$$\frac{\partial}{\partial t}\rho_{\mathrm{GS}}^j = -\frac{\left(\rho_{\mathrm{GS}}^j\right)^2}{\tau_{\mathrm{GS}}} + \widetilde{R}^{\mathrm{rel}}(j) - R_{\mathrm{GS}}^{j,\mathrm{stim}} \tag{3}$$

The inhomogeneous broadening of the QD states is modeled by a Gaussian density of states,

$$f^j = \mathcal{N}^{-1}\exp\left[-4\ln 2\left(\frac{\hbar\omega_{\mathrm{GS}}^j - E_{\mathrm{GS}}}{\Delta E_{\mathrm{inh}}^{\mathrm{GS}}}\right)^2\right], \tag{4}$$

with their respective center energies E_m and full-width-at-half-maximum $\Delta E_{\mathrm{inh}}^m$, as well as a normalization constant $\mathcal{N}$ ensuring $\sum_j f^j = 1$. The capture of charge carriers into the QD excited states is modeled by the net capture rate

$$\widetilde{R}_{\mathrm{ES}}^{\mathrm{cap}}(j) = R^{\mathrm{cap}}\left[F\left(\hbar\omega_{\mathrm{ES}}^j,\mu,T\right) - \rho_{\mathrm{ES}}^j\right], \tag{5}$$

with the quasi-Fermi function $F(E,\mu,T)$, where μ is the quasi-Fermi level in the carrier reservoir and T is the effective carrier temperature. Here, we neglect the direct capture into the QD GS for simplification. As the capture rate into the ES is usually the dominant contribution to the capture, and the intradot relaxation leads to a fast equilibration of GS and ES, this approximation still leads to reliable results. The corresponding net intradot relaxation rate is given by

$$\widetilde{R}^{\mathrm{rel}}(j) = R^{\mathrm{rel}}\left(1-\rho_{\mathrm{GS}}^j\right)\rho_{\mathrm{ES}}^j - R^{\mathrm{rel}}\rho_{\mathrm{GS}}^j\left(1-\rho_{\mathrm{ES}}^j\right)e^{-(\hbar\omega_{\mathrm{ES}}^j-\hbar\omega_{\mathrm{GS}}^j)/(k_BT)}, \tag{6}$$

with the last term being a Boltzmann factor ensuring relaxation towards quasiequilibrium. The stimulated recombination is included by

$$R_m^{j,\mathrm{stim}} = g\left(2\rho_m^j - 1\right)\mathcal{L}\left(\omega_m^j - \omega^{\mathrm{pump}}\right)S^{\mathrm{pump}}(t), \tag{7}$$

where g is the QD gain coefficient, $S^{\mathrm{pump}}(t)$ is the injected pump light intensity, and $\mathcal{L}(\omega) = \frac{T_2}{\pi}\,\mathrm{sech}(T_2\omega)$ is the homogeneous line-shape function, with the dephasing time T_2.

This model is used to simulate EL spectra (described in Appendix C) of the SK-QDs and shows excellent quantitative agreement with the experimental data (see Fig. 4). In order to fit the observed redshift of the EL peaks with increasing

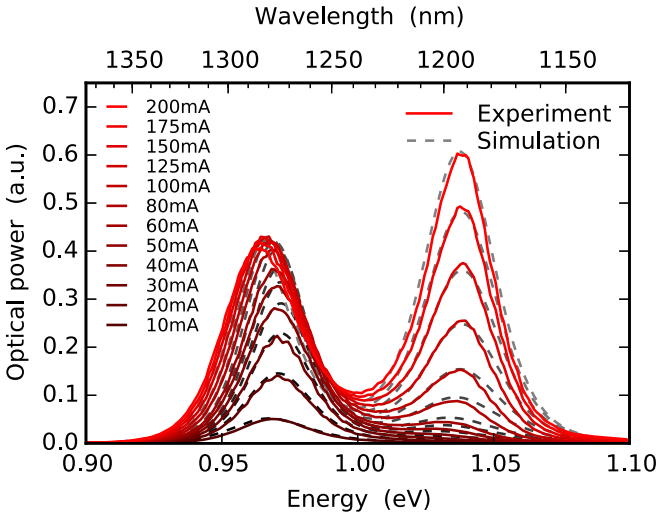

FIG. 4. Measured (solid lines) and calculated (dashed lines) emission spectra of the SK-QD device for a set of injection currents. The transparency current is $J_{tr} = 6$ mA.

current, we introduce a phenomenological linear shift of the transition energies,

$$\hbar\omega_m^j(J) = \hbar\omega_m^j(J=0) - 0.4\,\mathrm{meV}\frac{J}{J_{\mathrm{tr}}}, \tag{8}$$

where J_{tr} is the transparency current density. This shift accounts for the induced Varshni-shift by an increasing lattice temperature as well as band-gap shrinkage due to many-body Coulomb interaction [38]. Similarly, a decreasing dephasing time with pump current is assumed,

$$T_2(J) = \frac{T_2(J=0)}{\sqrt{1+0.05\frac{J}{J_{\mathrm{tr}}}}}, \tag{9}$$

accounting for more efficient dephasing processes with increasing carrier densities and temperature [39,40].

In addition to the static characteristics of the SK-QD amplifier device, the rate-equation model enables us to simulate its dynamic behavior under perturbation. We calculate the response to a Gaussian-shaped optical input pulse $S^{\mathrm{pump}}(t)$ with FWHM duration of 235 fs, which enters in the model in Eq. (7). The differential gain and phase recovery for a set of injection currents of the SK-QD SOA after optical perturbation resonantly to the QD ground state (GS) is plotted in Fig. 5. The experimental data is represented by open symbols; the calculated results are visualized by solid lines. An excellent agreement of the model and the measured gain recovery traces for injection currents below and above transparency is observed [Fig. 5(a)]. The experimental data allow us to extract the dynamic timescales of the internal carrier scattering processes. We find the carrier capture rate from the reservoir to be $R^{\mathrm{cap}} = 80\ \mathrm{ns}^{-1}$ and the intradot relaxation to be $R^{\mathrm{rel}} = 0.8\ \mathrm{ps}^{-1}$. The retrieved parameters for the model are listed in Table I. The comparison with our simulation results allows for an interpretation of the measured gain recovery curves. The characteristic time of roughly 100 ps, especially visible as a kink at low currents in Fig. 5(a), is directly related to the refilling of the QD states via carrier capture from the reservoir.

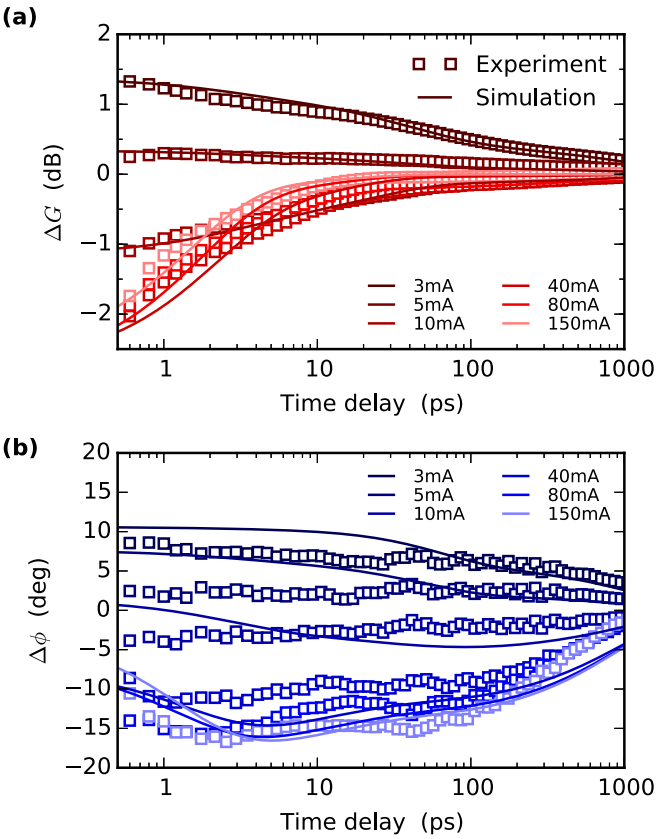

FIG. 5. (a) Measured (open symbols) and simulated (lines) gain recovery and (b) phase recovery curves of the SK-QD SOA after perturbation by an optical pump pulse. Shown are the results for different pump currents, with the transparency current being approximately 6 mA.

At higher currents, a pronounced bend at a time delay of 3 ps appears in the gain recovery, which we can attribute to the intradot relaxation. The QD ES acts as an additional carrier reservoir for the GS at elevated pump levels, leading to an ultrafast recovery of the GS gain.

In addition to changes in the gain, the carrier variation induced by the pump pulse leads to changes in the refractive index, which modifies the optical phase. Figure 5(b) shows the corresponding dynamics of the optical phase shift $\Delta\phi$ imprinted onto the probe pulse, which we calculate via the Kramers-Kronig relation (see Appendix C). We distinguish two sources of this phase change: off-resonant interband

TABLE I. Parameters as used in the simulations of the SK-QD device.

Symbol	Value	Symbol	Value
τ_{res}	1.2 ns	N^{QD}	$3\times10^{10}\ \mathrm{cm}^{-2}$
τ_{GS}	2 ns	$\Delta E_{\mathrm{inh}}^{\mathrm{GS}}$	40 meV
τ_{ES}	2.5 ns	$\Delta E_{\mathrm{inh}}^{\mathrm{ES}}$	55 meV
$E_{\mathrm{GS}}(J=0)$	0.976 eV	$E_{\mathrm{ES}}(J=0)$	1.056 eV
$E_g(J=0)$	1.086 eV	g	$16\times10^{-5}\ \mathrm{cm}^2\ \mathrm{ns}^{-1}$
R^{cap}	$80\ \mathrm{ns}^{-1}$	α_{int}	$75\ \mathrm{ns}^{-1}$
R^{rel}	$0.8\ \mathrm{ps}^{-1}$	$T_2(J=0)$	120 fs

transitions, i.e., from the ES and blue edge of the GS, lead to an asymmetric variation of the gain spectrum. The model does not explicitly describe effects such as free-carrier absorption or carrier heating, which are added phenomenologically via a linear dependence on the carrier densities [see Eq. (C5)]. Nevertheless, the dynamics of these processes is not accurately included in the model, which explains the observed deviation from the experimental data. Furthermore, the reservoir recovery time τ_{res} is assumed as constant in the simulations, for simplicity and to reduce the number of fit parameters. The observed recovery speed at long time delays is therefore underestimated in the simulations at elevated currents.

Compared to the gain recovery, the phase change of the SK-QDs can be seen to recover on a much longer timescale. This is due to the fact that the off-resonant ES and reservoir states are mainly responsible for the change in the refractive index. The ultrafast gain recovery of the GS is therefore always accompanied by a long-lived phase variation that recovers on the reservoir timescale. The strongly localized transitions of the SK-QD system, however, lead to a comparatively small phase change.

The comparison of simulation results with experimental data shows that our chosen rate-equation approach is suitable to describe the ultrafast gain recovery of QD SOAs. In the following, we will show that this modeling approach can be extended to the description of SML based amplifier devices.

B. Submonolayer quantum dots (SML-QDs)

The results presented in the previous section have shown that an accurate quantitative simulation of SK-QD amplifier devices is possible using the presented rate equation system. In our modeling of the SML-QD based amplifier structure we therefore pursue a similar theoretical approach. In contrast to the SK-QDs, we now assume a diffusive relaxation coupling between different dots, as sketched in Fig. 6. This is in line with predictions suggesting an effective carrier diffusion between neighboring SMLs [14]. Furthermore, this type of coupling does not require an explicit assumption about the nature of the relaxation, unlike in the case of SK-QDs, where each GS only couples to its corresponding ES. We modify the carrier reservoir to a three-dimensional one located at the GaAs band edge (see Fig. 1, right column). This is motivated by the current dependence of the changeover of the gain dynamics at ≈10 ps showing a quadratic dependence on the injection current, as has been predicted by numerical simulations of charge-carrier capture from a three-dimensional reservoir into zero-dimensional states [41].

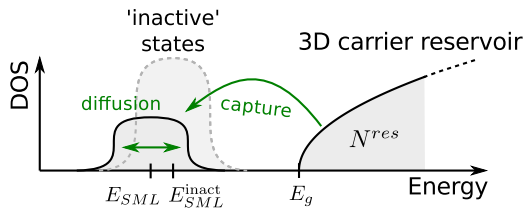

FIG. 6. Sketch of the density of states (DOS) assumed in the SML-QD rate equation model, along with the included scattering channels.

We therefore assume a current-dependent capture rate,

$$R_{\text{SML}}^{\text{cap}}(J) = 60\,\text{ns}^{-1}\left[\frac{J}{J_{\text{tr}}}\right]^2. \tag{10}$$

The rate equations for the SMLs coupled to a three-dimensional carrier reservoir are given by:

$$\frac{\partial}{\partial t}N^{\text{res}} = J - \frac{N^{\text{res}}}{\tau_{\text{res}}} - 2N^{\text{SML}}\sum_j f_{\text{SML}}^j \widetilde{R}_{\text{SML}}^{\text{cap}}(j) \tag{11}$$

$$\frac{\partial}{\partial t}\rho_{\text{SML}}^j = -\frac{\left(\rho_{\text{SML}}^j\right)^2}{\tau_{\text{SML}}} + \widetilde{R}_{\text{SML}}^{\text{cap}}(j) + \widetilde{R}_{\text{SML}}^{\text{rel}}(j) - R_{\text{SML}}^{j,\text{stim}} \tag{12}$$

with capture and relaxation rates

$$\widetilde{R}_{\text{SML}}^{\text{cap}}(j) = R_{\text{SML}}^{\text{cap}}(J)\left[F\left(\hbar\omega_{\text{SML}}^j,\mu,T\right) - \rho_{\text{SML}}^j\right] \tag{13}$$

$$\widetilde{R}_{\text{SML}}^{\text{rel}}(j) = \sum_{k\neq j} f^k\Big\{R_{\text{SML}}^{\text{rel}}\left(1-\rho_{\text{SML}}^j\right)\rho_{\text{SML}}^k - R_{\text{SML}}^{\text{rel}}\rho_{\text{SML}}^j\left(1-\rho_{\text{SML}}^k\right)e^{-(\hbar\omega_{\text{SML}}^k-\hbar\omega_{\text{SML}}^j)/(k_BT)}\Big\}. \tag{14}$$

The ultrafast carrier dynamics of the SML structure is governed by the interaction of the localized and three-dimensional subsystems. Obviously, the dimensionality of the carrier confinement influences the dynamics on different levels. In particular, a possibly different dimensionality for electrons and holes, as observed by Harrison *et al.* [21], can be largely ignored in the investigation of the ultrafast carrier dynamics. The long-range Coulomb interaction forces the delocalized carrier to follow its confined conjugate and makes it available for optical recombination. Even for the heteroconfinement of electrons and holes described above it is therefore adequate to limit our numerical description to an excitonic picture rather than treating electrons and holes separately.

To correctly model the dynamics of the SML SOA, an accurate representation of the DOS f^j has to be found, which we determine from the EL spectra. Taking into account the heteroconfinement various contributions would be imaginable. Thus, we simulate the EL spectra using the proposed SML rate equation model using parameters as given in Table II, but vary the shape of the SML DOS (insets in Fig. 7).

In Fig. 7(a) for the calculation of the EL spectra a Gaussian contribution as known from zero-dimensional structures has been implemented, similar to the inhomogeneous broadening assumed for SK-QDs. Whilst the peak emission is reproduced

TABLE II. Parameters as used in the simulations of the SML-QD device.

Symbol	Value	Symbol	Value
τ_{res}	2 ns	N^{SML}	3.3×10^{11} cm^{-2}
τ_{SML}	0.2 ns	$\Delta E_{\text{inh}}^{\text{SML}}$	30 meV
$E_{\text{SML}}(J=0)$	1.313 eV	$E_g(J=0)$	1.38 eV
$R_{\text{SML}}^{\text{cap}}$	Eq. (10)	$E_{\text{SML}}^{\text{inact}}(J=0)$	1.35 eV
$R_{\text{SML}}^{\text{rel}}$	15 ps^{-1}	α_{int}	75 ns^{-1}
$T_2(J=0)$	80 fs	g	15.4×10^{-5} cm^2 ns^{-1}

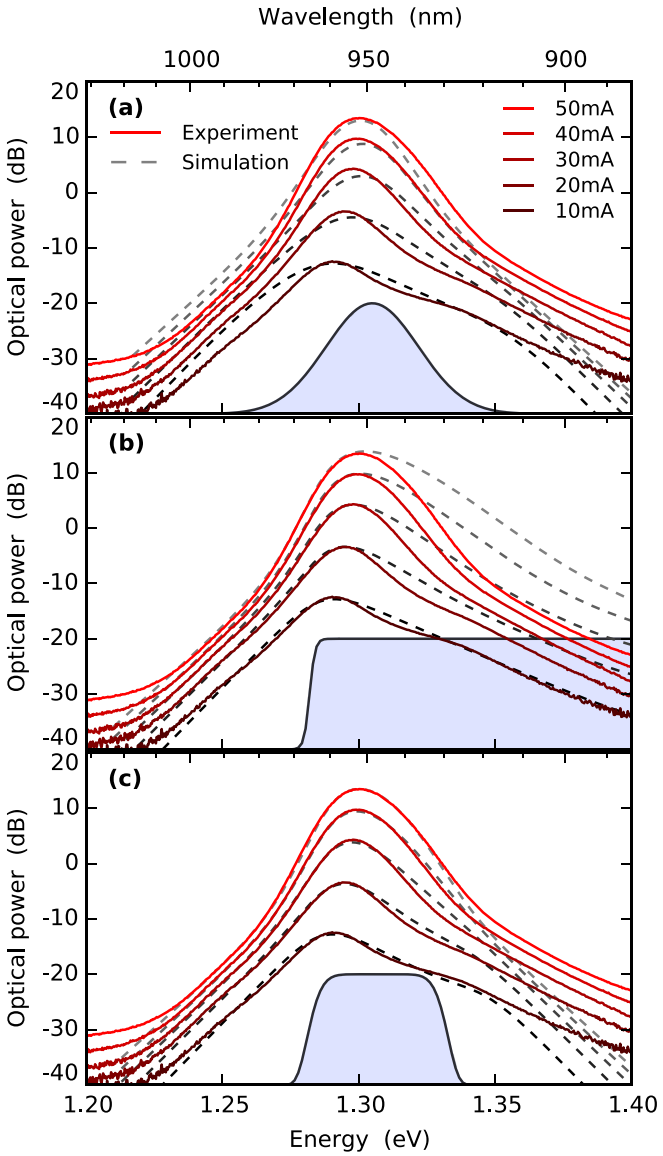

FIG. 7. Electroluminescence spectra for different densities of states (DOS) of the SML-QDs (shaded areas). Shown are the simulated (dashed lines) and measured (solid lines) spectra for different pump currents. (a) Inhomogeneously broadened 0D-like Gaussian DOS. (b) 2D-like constant DOS. (c) extended Gaussian DOS.

closely the high and low energy sides differ significantly, being over- and underestimated for low and high injection currents, respectively. Additionally the dip at around 1.31 eV is not reproduced either. Figure 7(b) shows the consideration of a two-dimensional-like DOS as known from QW devices, represented by a constant DOS and ending up with a Boltzmann tail on the low energy side of the spectrum. The peak emission as well as the red tail of the spectra are captured very well by this assumption. However, the blue side of the EL spectrum in this case is overestimated dramatically and the dip on the blue side qualitatively absent for low injection currents. Thus the failure of a purely two-dimensional DOS is obvious. Additionally, in photoluminescence excitation experiments performed using a Ti:sapphire pump laser ranging from 880 nm to 970 nm excitation wavelength no luminescence at the SML GS has been found for wavelengths shorter than 940 nm, thus proving the absence of additional reservoir states in this wavelength range.

To reproduce both the sharp decay on the red side and the longer tail on the blue side, we test the distribution shown in Fig. 7(c),an extended Gaussian-distributed DOS, which shows the overall best fit to the EL spectra. This DOS is implemented via

$$f^k = \mathcal{N}^{-1} \exp\left[-4\ln 2\left(\frac{\hbar\omega^k_{\mathrm{SML}} - E_{\mathrm{SML}}}{\Delta E^{\mathrm{SML}}_{\mathrm{inh}}}\right)^8\right], \qquad (15)$$

combining the localized character of zero-dimensional structure and the nearly constant DOS of two-dimensional systems. A physical explanation of this DOS could be that the 2D-delocalized electrons associated with a hole state contribute the typical flat 2D energy distribution up to a certain threshold value when the kinetic energy exceeds the Coulomb forces forming the exciton. The high energy side of the spectrum is slightly underestimated using this DOS, suggesting that there exists a small number of optically active states at these energies. Our numerical simulations, however, show that their DOS can be at most 10% of the DOS around the emission peak, otherwise the EL response would be greatly overestimated, as seen in panel (b).

In Fig. 7 a strong increase of the EL peak intensity of nearly 25 dB upon an increase of the pump current from 10 mA to 50 mA can be observed. From the simulations at 10 mA we extract a modal gain of −6 dB (below transparency) at 960 nm, which increases to 20 dB at 40 mA. This is much higher than what we observe for the SK-QD SOA device (13 dB modal gain at 200 mA), owing to the high density of states in the SML-QD medium.

We proceed by simulating the dynamic recovery of the SML-QD device. Analogous to the previous case we perturb the SML-QD gain medium by a strong pump pulse and calculate the time-dependent recovery of the modal gain and phase shift. The resulting curves are shown in Fig. 8(a) together with the experimentally acquired data. The simulation results reproduce the measurements closely. We attribute the ultrafast sub-ps gain recovery to the diffusive relaxation process between different SML states and choose the corresponding relaxation rate in accordance with the observed timescale. In order to explain the initial gain recovery, an efficient, ultrafast refilling of the active SML states must be implemented. To this end, we include an additional inactive portion $f^{\mathrm{SML,inact}} = 0.76$ of "dark" SML states into the DOS distribution as an effective energy level at an energy of $E^{\mathrm{inact}}_{\mathrm{SML}}$. We define those states as "dark" which do not contribute to the light-matter interaction, i.e., their transition matrix element is negligible. This means that nearly three quarters of the carriers do not contribute to the optical gain and stimulated emission processes but act as an additional carrier reservoir for the refilling of active SML states, coupled via the diffusive relaxation process introduced in Eq. (12). Those dark states are formed by either free carriers or excitons outside the radiative cone. In the model equations, the inactive states enter as an additional subgroup f^{inact}, without the stimulated emission contribution $R^{j,\mathrm{stim}}_{\mathrm{SML}}$. It is important to note that these

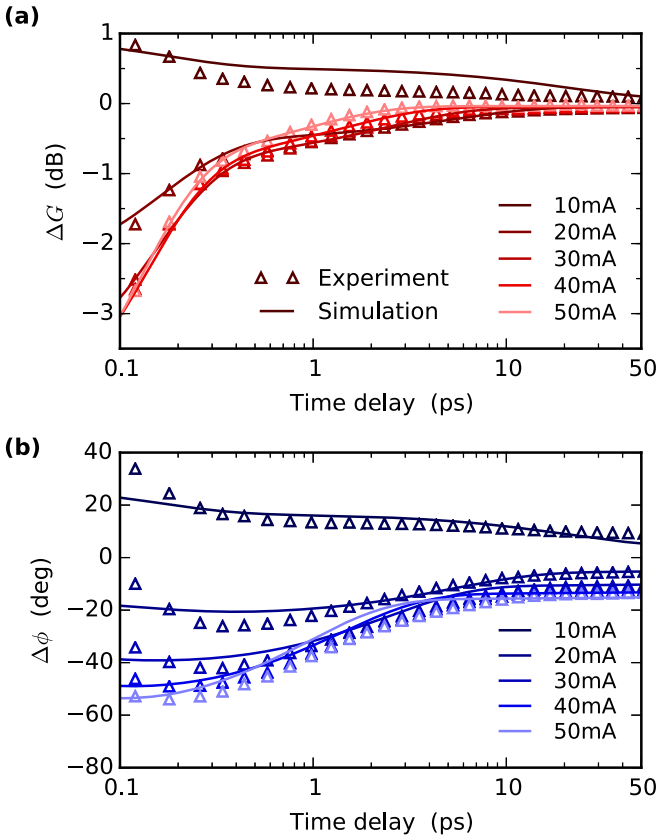

FIG. 8. (a) Measured (open symbols) and simulated (lines) gain recovery and (b) phase recovery curves of the SML-QD SOA after perturbation by an optical pump pulse. Shown are the results for different pump currents, with the transparency current being approximately 13 mA. Cf. Fig. 5.

inactive states do not exhibit an optical transition near the SML energies. This becomes evident from the EL spectra, where such a high number of states would appear as a strong EL signal. Nevertheless, these states are crucial for the ultrafast gain recovery of the SML transition.

The recovery of the optical phase is shown in Fig. 8(b). As before, the dynamic charge carrier timescales strongly determine the shape of the recovery curves. On the sub-ps timescale the phase change is built up due to the perturbation of the reservoir states. Here we can see that even though the inactive SML states do not influence the optical gain, they induce a strong optical phase shift. Around 10 ps, the phase partially recovers due to the capture of carriers from the bulk reservoir into the SML states. Clearly visible is the quadratic reduction of the capture time with current from around 20 ps below transparency to a few ps at 50 mA. As explained above, this is evidence for three-dimensional bulk states acting as a carrier reservoir for the system.

C. Optically inactive SML states

The comparison between experimental and numerical results shows that the fast part of the gain recovery is excellently described by a capture of carriers from neighboring localization centers with a rate of 15 ps^{-1}. Although we find a large optical gain in the evaluation of the EL spectra, most of

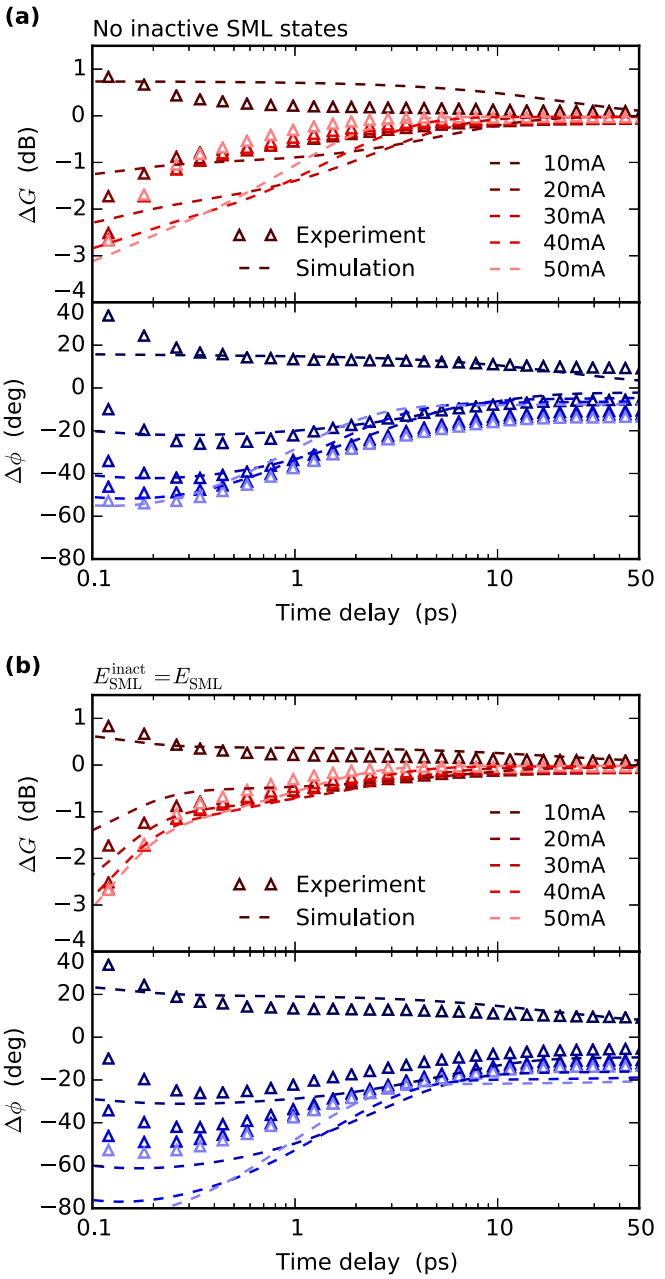

FIG. 9. (a) Simulated SML gain and phase recovery without the inclusion of inactive SML-QD states. The ultrafast gain recovery is absent without the coupling to the carriers in the optically inactive states. (b) Simulation without an energy spacing between the SML ensemble and the effective "dark" state level. The inaccurate current dependence especially of the gain recovery shows the importance of the energetic position of the inactive states. Cf. Fig. 8.

the localization centers have to be assumed as optically inactive at the probe wavelength to account for the highly efficient gain recovery below 1 ps. The effect on the gain dynamics of these states is depicted in Fig. 9(a). Only having a fourfold excess of "dark" SMLs quantitatively explains the initial gain recovery but also entails a large differential phase change.

The results of photoluminescence and magneto-optical experiments reported in the literature show a combination of 0D and 2D features in the SML emission; some of the authors

suggest a coexistence of localized holes and delocalized electrons in these structures [21,22]. Under these conditions, not all carriers are correlated in excitons, which can then resonantly interact with the applied light field. In our SML structure, there seems to be a threshold energy, beyond which the formation of excitons is impossible, reflected in a steeply decaying DOS for the optically active states at high energy. The numerical simulations of gain and phase recovery, on the other hand, show that there is a reservoir of carriers, the so-called "dark" states, beyond the exciton limit energy. This reservoir is most probably formed by uncorrelated electrons and holes.

The exact shape of the assumed "dark" states cannot be deduced from our results due to the absence of an optical signature. In our modeling, these states therefore enter only as an effective level with a high density of states at an energy $E_{\mathrm{SML}}^{\mathrm{inact}}$. Our results suggest that these states lie energetically higher by about 40 meV than the observed EL peak. This energy spacing between the active and inactive states is important for the quantitative modeling of the gain recovery. The energy of the inactive states relative to the quasi-Fermi level determines the number of carriers available for the ultrafast recovery and thus strongly influences its current dependence. This effect is illustrated in Fig. 9(b), where the energy spacing between active and inactive SML states was set to zero. The agreement with the experimental data in this case is significantly worse. We therefore conclude that the initial gain recovery is dominated by a refilling of the SML states by energetically higher states. Taking into account the considerations by Harrison *et al.* [21], this might hint towards the delocalized carriers acting as an additional charge-carrier reservoir for the optically active states. At the present point the exact nature of these states, however, cannot be deduced and therefore needs to be addressed in future works.

IV. CONCLUSIONS

We have investigated the ultrafast gain and phase recovery of an SML SOA in pump-probe experiments and numerical simulations and compared the results to observations on an SOA based on standard SK-QDs in a DWELL structure. The numerical model we developed gives an insight into the processes dominating the carrier dynamics in SML structures and allows us to extract similarities and differences between the shallow-confining localization centers in SMLs and the strongly confining self-assembled QDs. We find a gain of 90 cm^{-1} at $J = 4J_{\mathrm{tr}}$, which exceeds by far the gain of SK-QD based active regions. The high density of localization centers thus translates into a high density of available optical power. The numerical modeling, however, shows that still most of the localization centers in the SML sample are optically inactive.

SMLs display a fast and efficient gain recovery on the ps timescale, being as fast as for the SK-QDs. In the case of SMLs this efficient carrier reservoir is formed by the optically inactive localization centers, rather than an additional 2D reservoir as in DWELL structures. This is clearly shown by the quadratic current dependence of the gain recovery rate. While the bulk sates act as a slow carrier reservoir for the SML carriers, the coupling of the localization centers with the optically inactive states is the dominating recovery mechanism at short times. Unlike for SK-QD DWELL structures, it is therefore not necessary to introduce an additional reservoir layer. The presence of an intrinsic carrier reservoir in the SML structures has the advantage of incorporating less sources of defects during the growth process.

While the optically inactive states provide a fast and strong gain recovery channel, their presence also entails a large differential change in the refractive index. This leads to a significant nonlinear index change of the SML device, exhibiting a more than tenfold higher phase change compared to the SK-QD medium. An active medium based on SMLs thus offers very favorable properties for nonlinear optoelectronics applications employing self or cross-phase modulation.

ACKNOWLEDGMENTS

We are grateful to J.-H. Schulze, A. Strittmatter, and U. Pohl for discussions and the growth of the SML structure. Both QD SOAs were processed in the group of D. Bimberg. Financial support was provided by Deutsche Forschungsgemeinschaft (DFG) via Sonderforschungsbereich 787 and the Research Training Group 1558.

APPENDIX A: DEVICE DETAILS

1. SML SOA

Five layers of SMLs are formed by sixfold depositions of alternately 0.4 monolayers (MLs) InAs and 1.6 ML GaAs, being separated by 40 ML GaAs spacers. Scanning electron microscopy images of a similar structure show that this growth mode generates In-rich agglomeration centers with an areal density of about 10^{12} cm^{-2}, a lateral size of 5 nm, and a height of several monolayers, which is comparable to small self-assembled grown QDs [42].

The active region is sandwiched in a p-side-up pin structure to allow for current injection and processed into an edge-emitting SOA structure. The 0.5 mm long waveguide is shallow etched down to ≈80 nm above the active region along a ridge of 2 μm width, and the as-cleaved facets are tilted eight degrees against the normal to suppress feedback into the cavity. The temperature of the sample is stabilized by water cooling.

2. SK-QD SOA

The active region contains 15 layers of self-assembled QDs grown by molecular beam epitaxy with a nominal QD density of $N^{\mathrm{QD}} = 5 \times 10^{10}$ cm^{-2}. The QDs are immersed in an InGaAs QW in a DWELL structure. The QD layers are separated by 33–35 nm thick GaAs barriers to prevent vertical coupling. The active region is enclosed between p and n doped bulk GaAs (pin structure). The lateral extension of the active region is 2 μm; the length of the waveguide is 1.5 mm.

APPENDIX B: HETERODYNE PUMP-PROBE EXPERIMENT

Pump and probe laser pulses are generated by a Toptica FemtoFiber Pro laser system, in which an amplified Er-doped fiber oscillator running with a repetition rate of 75.4 MHz at a wavelength of 1550 nm seeds two independently tunable highly nonlinear fibers, which generate spectral supercontinua

from which suitable portions are cut by amplitude masks in the Fourier plane of pulse shapers. The resulting laser pulses are compressed to < 250 fs full width at half maximum (FWHM) duration, with the pulse powers typically about 300 μW for the pump and 30 μW for the probe pulse. Acousto-optical modulators (AOMs) in the pump and probe paths are used to rapidly adjust intensities. Fast switching of the pump pulse intensity allows us to quasisimultaneously record data at different pump pulse powers to control the influence of nonlinear processes on the sample dynamics. Additionally, the nondeflected part of the probe beam is used as a reference beam in the balanced heterodyne detection scheme. The beating pattern at 1.9 MHz generated by superimposing probe and reference beams on a fast detector (New Focus 2117) is then analyzed in amplitude and phase by a fast lock-in amplifier (Perkin Elmer DSP7280).

APPENDIX C: CALCULATION OF EL SPECTRA AND GAIN

We calculate the EL spectra under small-signal assumptions. Along the waveguide axis z the propagation of the EL signal at the optical excitation frequency ω is determined by a constant spontaneous emission source term and the optical gain:

$$\frac{\mathrm{d}}{\mathrm{d}z} S_{EL}(\omega,z) = R_{EL}(\omega) + \mathcal{G}(\omega) S_{EL}(\omega,z)\,, \tag{C1}$$

which can be integrated along the device length ℓ, giving the EL intensity at the output facet,

$$S_{EL}(\omega,\ell) = R_{EL}(\omega)\frac{e^{\mathcal{G}(\omega)\ell}-1}{\mathcal{G}(\omega)}\,. \tag{C2}$$

The spontaneous emission rate is determined from the contributions of all active transitions:

$$R_{EL}(\omega) \propto \sum_m N^m \sum_j f^j \frac{\left(\rho_m^j\right)^2}{\tau_m} \mathcal{L}\left(\omega-\omega_m^j\right), \tag{C3}$$

TABLE III. Phase change coefficients used in the simulation of the carrier-induced phase shift.

SK-QDs		SMLs	
Symbol	Value	Symbol	Value
$\delta\phi^{\mathrm{GS}}$	0	$\delta\phi^{\mathrm{SML}}$	0
$\delta\phi^{\mathrm{ES}}$	6.3×10^{-10} cm	$\delta\phi^{\mathrm{SML,inact}}$	2.2×10^{-9} cm
$\delta\phi^{\mathrm{res}}$	2.5×10^{-9} cm	$\delta\phi^{\mathrm{res}}$	5.6×10^{-10} cm

where $\mathcal{L}$ is the line-shape function and $N^m = \{2N^{\mathrm{QD}}, 4N^{\mathrm{QD}}, 2N^{\mathrm{SML}}\}$ for GS, ES, and SML, respectively. The modal gain $\mathcal{G}(\omega)$ is calculated analogously,

$$\mathcal{G}(\omega) = \frac{g}{v_g}\sum_m N^m \sum_j f^j\left(2\rho_m^j - 1\right)\mathcal{L}\left(\omega-\omega_m^j\right) - \alpha_{\mathrm{int}} \tag{C4}$$

with internal losses $\alpha_{\mathrm{int}} = 10\ \mathrm{cm}^{-1}$. The induced phase change after propagation through the device is calculated from the Kramers-Kronig relation,

$$\Delta\phi(\omega) = \frac{2\ell}{\pi}\int \frac{\mathcal{G}(\omega')}{\omega'-\omega}\mathrm{d}\omega' + \ell\sum_m \delta\phi^m N^m\,, \tag{C5}$$

where the second term is a phenomenological contribution describing index changes induced by effects other than the modeled intraband transitions, such as free-carrier absorption. The summation index m runs over the QD GS, ES, and reservoir states in the case of SK-QDs, or over the SML, inactive SML, and reservoir states in the case of the SML device. The phase change coefficients are given in Table III, which were fitted to reproduce the measured data.

[1] M. Grundmann, O. Stier, and D. Bimberg, InAs/GaAs pyramidal quantum dots: Strain distribution, optical phonons, and electronic structure, Phys. Rev. B **52**, 11969 (1995).

[2] Y. Todorov, A. M. Andrews, R. Colombelli, S. De Liberato, C. Ciuti, P. Klang, G. Strasser, and C. Sirtori, Ultrastrong Ligh-Matter Coupling Regime with Polariton Dots, Phys. Rev. Lett. **105**, 196402 (2010).

[3] *Quantum Optics with Semiconductor Nanostructures*, edited by F. Jahnke (Woodhead, Cambridge, 2012).

[4] *Nano-Optoelectronics: Concepts, Physics and Devices*, edited by M. Grundmann (Springer, Berlin, 2002).

[5] P. M. Petroff, *Single Quantum Dots: Fundamentals, Applications and New Concepts*, edited by P. Michler (Springer, Berlin, 2003).

[6] M. S. Skolnick and D. J. Mowbray, Self-assembled semiconductor quantum dots: Fundamental physics and device applications, Annu. Rev. Mater. Res. **34**, 181 (2004).

[7] T. W. Berg and J. Mørk, Saturation and noise properties of quantum-dot optical amplifiers, IEEE J. Quantum Electron. **40**, 1527 (2004).

[8] J. Gomis-Bresco, S. Dommers, V. V. Temnov, U. Woggon, M. Laemmlin, D. Bimberg, E. Malic, M. Richter, E. Schöll, and A. Knorr, Impact of Coulomb Scattering on the Ultrafast Gain Recovery in InGaAs Quantum Dots, Phys. Rev. Lett. **101**, 256803 (2008).

[9] N. A. Cherkashin, M. V. Maksimov, A. G. Makarov, V. A. Shchukin, V. M. Ustinov, N. V. Lukovskaya, Yu. G. Musikhin, G. E. Cirlin, N. A. Bert, Zh. I. Alferov, N. N. Ledentsov, and D. Bimberg, Control over the parameters of inas-gaas quantum dot arrays in the stranski-krastanov growth mode, Semiconductors **37**, 861 (2003).

[10] S. Krishna, D. Zhu, J. Xu, K. K. Linder, O. Qasaimeh, P. Bhattacharya, and D. L. Huffaker, Structural and luminescence characteristics of cycled submonolayer inas/gaas quantum dots

with room-temperature emission at 1.3 μm, J. Appl. Phys. **86**, 6135 (1999).

[11] T. Niermann, F. Kießling, M. Lehmann, J.-H. Schulze, T. D. Germann, K. Pötschke, A. Strittmatter, and U. W. Pohl, Atomic structure of closely stacked inas submonolayer depositions in gaas, J. Appl. Phys. **112**, 083505 (2012).

[12] D. Arsenijević, C. Liu, A. Payusov, M. Stubenrauch, and D. Bimberg, Temperature-dependent characteristics of single-mode InAs submonolayer quantum-dot lasers, IEEE Photonics Technol. Lett. **24**, 906 (2012).

[13] P. Qiao, C. Y. Lu, D. Bimberg, and S. L. Chuang, Theory and experiment of submonolayer quantum-dot metal-cavity surface-emitting microlasers, Opt. Express **21**, 30336 (2013).

[14] B. Herzog, N. Owschimikow, J.-H. Schulze, R. Rosales, Y. Kaptan, M. Kolarczik, T. Switaiski, A. Strittmatter, D. Bimberg, U. W. Pohl, and U. Woggon, Fast gain and phase recovery of semiconductor optical amplifiers based on submonolayer quantum dots, Appl. Phys. Lett. **107**, 201102 (2015).

[15] D. Z.-Y. Ting, S. V. Bandara, S. D. Gunapala, J. M. Mumolo, S. A. Keo, C. J. Hill, J. K. Liu, E. R. Blazejewski, S. B. Rafol, and Y.-C. Chang, Submonolayer quantum dot infrared photodetector, Appl. Phys. Lett. **94**, 111107 (2009).

[16] P. Lam, J. Wu, M. Tang, Q. Jiang, S. Hatch, R. Beanland, J. Wilson, R. Allison, and H. Liu, Submonolayer InGaAs/GaAs quantum dot solar cells, Sol. Energ. Mat. Sol. **126**, 83 (2014).

[17] Z. C. Xu, K. Leosson, D. Birkedal, V. Lyssenko, J. M. Hvam, and J. Sadowski, InGaAs/GaAs quantum-dot–quantum-well heterostructure formed by submonolayer deposition, Nanotechnology **14**, 1259 (2003).

[18] L. C. Andreani, G. Panzarini, and J.-M. G´erard, Strong-coupling regime for quantum boxes in pillar microcavities: Theory, Phys. Rev. B **60**, 13276 (1999).

[19] Z. C. Xu, Y. T. Zhang, J. M. Hvam, J. J. Xu, X. S. Chen, and W. Lu, Carrier dynamics in submonolayer InGaAs/GaAs quantum dot, Appl. Phys. Lett. **89**, 013113 (2006).

[20] A. Manohar, S. Sengupta, H. Ghadi, and S. Chakrabarti, A detailed study of the effects of rapid thermal annealing on the luminescence properties of inas sub-monolayer quantum dots, J. Lumin. **158**, 149 (2015).

[21] S. Harrison, M. P. Young, P. D. Hodgson, R. J. Young, M. Hayne, L. Danos, A. Schliwa, A. Strittmatter, A. Lenz, H. Eisele, U. W. Pohl, and D. Bimberg, Heterodimensional charge-carrier confinement in stacked submonolayer InAs in GaAs, Phys. Rev. B **93**, 085302 (2016).

[22] D. Quandt, J.-H. Schulze, A. Schliwa, Z. Diemer, C. Prohl, A. Lenz, H. Eisele, A. Strittmatter, U. W. Pohl, M. Gschrey, S. Rodt, S. Reitzenstein, D. Bimberg, M. Lehmann, and M. Weyland, Strong charge-carrier localization in InAs/GaAs submonolayer stacks prepared by Sb-assisted metalorganic vapor-phase epitaxy, Phys. Rev. B **91**, 235418 (2015).

[23] N. Owschimikow, M. Kolarczik, Y. Kaptan, Nicolai B. Grosse, and U. Woggon, Crossed excitons in a semiconductor nanostructure of mixed dimensionality, Appl. Phys. Lett. **105**, 101108 (2014).

[24] P. Borri, W. Langbein, J. Mørk, and J.M. Hvam, Heterodyne pump-probe and four-wave mixing in semiconductor optical amplifiers using balanced lock-in detection, Opt. Commun. **169**, 317 (1999).

[25] M. Kolarczik, N. Owschimikow, B. Herzog, F. Buchholz, Y. I. Kaptan, and U. Woggon, Exciton dynamics probe the energy structure of a quantum dot-in-a-well system: The role of Coulomb attraction and dimensionality, Phys. Rev. B **91**, 235310 (2015).

[26] Y. Kaptan, A. Röhm, B. Herzog, B. Lingnau, H. Schmeckebier, D. Arsenijević, V. Mikhelashvili, O. Schöps, M. Kolarczik, G. Eisenstein, D. Bimberg, U. Woggon, N. Owschimikow, and K. Lüdge, Stability of quantum-dot excited-state laser emission under simultaneous ground-state perturbation, Appl. Phys. Lett. **105**, 191105 (2014).

[27] T. Vallaitis, C. Koos, R. Bonk, W. Freude, M. Laemmlin, C. Meuer, D. Bimberg, and J. Leuthold, Slow and fast dynamics of gain and phase in a quantum dot semiconductor optical amplifier. Opt. Express **16**, 170 (2008).

[28] X. Huang, X. H. Zhang, Y. G. Zhu, T. Li, L. F. Han, X. J. Shang, H. Q. Ni, and Z. C. Niu, The refractive nonlinearities of InAs/GaAs quantum dots above-bandgap energy, Opt. Commun. **283**, 1510 (2010).

[29] H. Zhang, S. Virally, Q. Bao, L. Kian Ping, S. Massar, N. Godbout, and P. Kockaert, Z-scan measurement of the nonlinear refractive index of graphene, Opt. Lett. **37**, 1856 (2012).

[30] A. Röhm, B. Lingnau, and K. Lüdge, Ground-state modulation-enhancement by two-state lasing in quantum-dot laser devices, Appl. Phys. Lett. **106**, 191102 (2015).

[31] B. Lingnau, W. W. Chow, E. Schöll, and K. Lüdge, Feedback and injection locking instabilities in quantum-dot lasers: a microscopically based bifurcation analysis, New J. Phys. **15**, 093031 (2013).

[32] Y. Kaptan, H. Schmeckebier, B. Herzog, D. Arsenijević, M. Kolarczik, V. Mikhelashvili, N. Owschimikow, G. Eisenstein, D. Bimberg, and U. Woggon, Gain dynamics of quantum dot devices for dual-state operation, Appl. Phys. Lett. **104**, 261108 (2014).

[33] T. R. Nielsen, P. Gartner, and F. Jahnke, Many-body theory of carrier capture and relaxation in semiconductor quantum-dot lasers, Phys. Rev. B **69**, 235314 (2004).

[34] K. Lüdge, *Nonlinear Laser Dynamics - From Quantum Dots to Cryptography*, edited by K. Lüdge (Wiley-VCH, Weinheim, 2012).

[35] M. Borgstrom, T. Bryllert, T. Sass, B. Gustafson, L. E. Wernersson, W. Seifert, and L. Samuelson, High peak to valley ratios observed in InAs/InP resonant tunneling quantum dot stacks, Appl. Phys. Lett. **78**, 3232 (2001).

[36] I. O'Driscoll, T. Piwonski, C. F. Schleussner, J. Houlihan, G. Huyet, and R. J. Manning, Electron and hole dynamics of InAs/GaAs quantum dot semiconductor optical amplifiers, Appl. Phys. Lett. **91**, 071111 (2007).

[37] N. Majer, S. Dommers-Völkel, J. Gomis-Bresco, U. Woggon, K. Lüdge, and E. Schöll, Impact of carrier-carrier scattering and carrier heating on pulse train dynamics of quantum dot semiconductor optical amplifiers, Appl. Phys. Lett. **99**, 131102 (2011).

[38] W. W. Chow and S. W. Koch, Theory of semiconductor quantum-dot laser dynamics, IEEE J. Quantum Electron. **41**, 495 (2005).

[39] T. Koprucki, A. Wilms, A. Knorr, and U. Bandelow, Modeling of quantum dot lasers with microscopic treatment of Coulomb effects, Opt. Quantum Electron. **42**, 777 (2011).

[40] E. Goldmann, M. Lorke, Th. Frauenheim, and F. Jahnke, Negative differential gain in quantum dot systems: Interplay of structural properties and many-body effects, Appl. Phys. Lett. **104**, 242108 (2014).

[41] A. Wilms, D. Breddermann, and P. Mathé, Theory of direct capture from two- and three-dimensional reservoirs to quantum dot states, Phys. Status Solidi C **9**, 1278 (2012).

[42] A. Lenz, H. Eisele, J. Becker, J.-H. Schulze, T. D. Germann, F. Luckert, K. Pötschke, E. Lenz, L. Ivanova, A. Strittmatter, D. Bimberg, U. W. Pohl, and M. Dähne, InAs/GaAs submonolayer quantum dot superluminescent diode emitting around 970 nm, J. Vac. Sci. Technol. B **29**, 04D104 (2011).